The Journal of
Physical Chemistry
Letters

Letter

Cite This: J. Phys. Chem. Lett. 2018, 9, 6144−6148

pubs.acs.org/JPCL

Anomalous Exciton Quenching in Organic Semiconductors in the Low-Yield Limit

Nasim Zarrabi,[†] Aren Yazmaciyan,[§] Paul Meredith,[*,†] Ivan Kassal,[*,‡] and Ardalan Armin[*,†]

[†]Department of Physics, Swansea University, Singleton Park, Swansea, Wales SA2 8PP, United Kingdom
[‡]School of Chemistry and the University of Sydney Nano Institute, The University of Sydney, Sydney, NSW 2006, Australia
[§]School of Mathematics and Physics, The University of Queensland, St. Lucia, QLD 4072, Australia

Supporting Information

ABSTRACT: The dynamics of exciton quenching are critical to the operational performance of organic optoelectronic devices, but their measurement and elucidation remain ongoing challenges. Here, we present a method for quantifying small photoluminescence quenching efficiencies of organic semiconductors under steady-state conditions. Exciton quenching efficiencies of three different organic semiconductors, PC70BM, P3HT, and PCDTBT, are measured at different bulk quencher densities under continuous low-irradiance illumination. By implementing a steady-state bulk-quenching model, we determine exciton diffusion lengths for the studied materials. At low quencher densities we find that a secondary quenching mechanism is in effect, which is responsible for approximately 20% of the total quenched excitons. This quenching mechanism is observed in all three studied materials and exhibits quenching volumes on the order of several thousand cubic nanometers. The exact origin of this quenching process is not clear, but it may be indicative of delocalized excitons being quenched prior to thermalization.

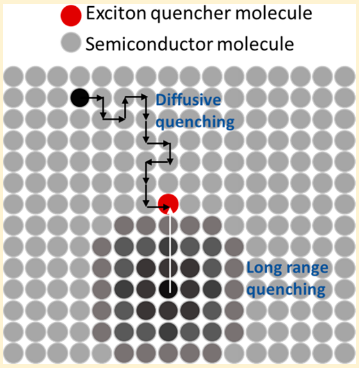

Organic semiconductors are generally disordered materials with low permittivities and strongly bound photoexcitations (excitons) at room temperature.[1,2] Exciton migration and the associated dynamics play important roles in defining the performance of organic optoelectronic devices, including organic solar cells (OSCs), organic light emitting diodes (OLEDs), organic photodetectors (OPDs), and sensors operating based on exciton quenching.[3−6] Exciton migration through organic semiconductors is diffusive, usually described by site-to-site hopping of localized excitons. Significant effort has been expended to evaluate the diffusion lengths of singlet excitons in particular because they are the more prevalent species.[7−11] In this regard, exciton diffusion lengths are often evaluated by studying the dynamics of exciton quenching in the presence of quenchers; specifically, time-resolved photoluminescence (PL) measurements can evaluate exciton lifetimes and diffusion coefficients, providing sufficient information to infer the exciton diffusion lengths.[12−17]

However, the signal-to-noise-ratio (SNR) of PL quenching measurements approaches zero at low quenching efficiencies because of the background noise, which contains sample-to-sample variation and photon shot noise in low-emissive-yield systems. It has therefore been very challenging to quantify small exciton quenching yields, a problem recently addressed by Siegmund et al.,[18] using one-dimensional (1-D) modeling of solar cell photocurrent spectra to extract exciton diffusion lengths even in nonfluorescent materials.

To investigate exciton quenching at low quencher densities (i.e., in the low-yield limit), we developed a method for measuring exciton quenching efficiencies under steady-state conditions using low-irradiance thermal light. The technique relies upon a steady-state three-dimensional (3-D) quenching model that can be fitted to experimental results to directly quantify exciton diffusion lengths, with no requirement for knowledge of the exciton lifetimes and diffusion coefficients. Importantly, because our method is background-free, i.e., it is sensitive only to the quenched part of the PL signal, it remains accurate at low quenching efficiencies. In this regime, we observe an anomalous exciton quenching pathway that is absent at high yields and would not be observed in transient measurements. This secondary quenching pathway corresponds to large quenching volumes and may originate from the quenching of delocalized excitons prior to thermalization.[19−22]

Steady-State Bulk Quenching Model. The quenching efficiency can be related to the quencher density without solving the diffusion equation as follows: We consider a molecular semiconductor matrix slightly doped with an exciton quenching material, so that the ith quencher molecule is located at position $\mathbf{r}_i$. We denote the probability that an exciton initially at $\mathbf{r}$ will be quenched at quencher i as $p(|\mathbf{r} - \mathbf{r}_i|)$, for a monotonically decreasing function $p(r)$. The probability that the exciton is quenched by any of the N quenchers within the matrix is then $1 - \prod_{i=1}^{N}(1 - p(|\mathbf{r} - \mathbf{r}_i|))$. The observable quenching yield (QY) is obtained by averaging the quenching probability over the initial position of the exciton:

Received: August 13, 2018
Accepted: October 5, 2018
Published: October 5, 2018

ACS Publications

DOI: 10.1021/acs.jpclett.8b02484
J. Phys. Chem. Lett. 2018, 9, 6144−6148

$$\mathrm{QY} = \frac{1}{V}\iiint_V \left[1 - \prod_{i=1}^{N}\left(1 - p(|\mathbf{r} - \mathbf{r}_i|)\right)\right]\mathrm{d}\mathbf{r} \tag{1}$$

The QY increases linearly with the quencher density at low densities, where the quenching volumes of individual quenchers do not overlap. It deviates from linearity with increasing quencher density until saturation is achieved, where the whole space is covered by the quenching volumes (Figure 1).

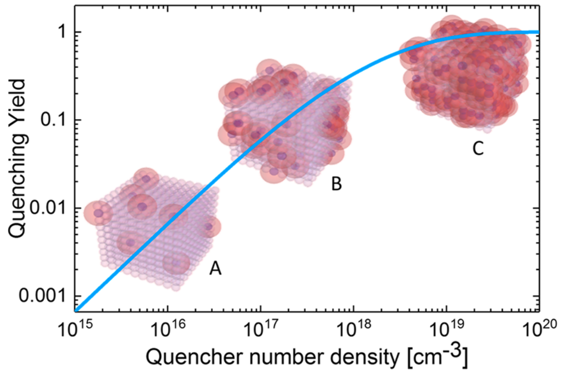

Figure 1. Exciton quenching yield versus quencher number density under steady-state conditions. Each quencher is surrounded by a sphere indicating its quenching volume. At low densities, increasing the number of quenchers results in a linear increase in the quenching yield. A deviation from linearity occurs as the quenching volumes start overlapping. Ultimately, the whole space is quenched, and a saturation is achieved.

To compute the QY, we first determine $p(r)$ by assuming a quencher of radius a centered at the origin of a 1-D lattice with lattice constant δ. The exciton undergoes a random walk with lifetime τ and is quenched if found at the position $x = a$. The probability $p(x)$ obeys the following relation:

$$p(x) = \frac{1}{2}(p(x - \delta) + p(x + \delta)) - \frac{\Delta t}{\tau}p(x) \tag{2}$$

where Δt is the time of each jump. The first, lossless term indicates that the survival probability for a walker starting at x equals the average of the probabilities for a walker starting from the points reachable in one step from x. The second term adds loss, i.e., some probability is lost during each jump to ensure an exponential decay with lifetime τ. From the definition of the second derivative, in the continuum limit ($\delta \to 0$) eq 2 becomes

$$\frac{\mathrm{d}^2}{\mathrm{d}x^2}p(x) - \frac{2\Delta t}{\delta^2\tau}p(x) = 0 \tag{3}$$

where $\delta^2/2\Delta t$ equals the diffusion constant D (in one dimension). In three dimensions, this becomes the spherically symmetric Helmholtz equation:

$$\nabla^2 p(\mathbf{r}) - \frac{1}{D\tau}p(\mathbf{r}) = 0 \tag{4}$$

whose radial part is solved by a spherical Bessel function of order zero. In particular, the real solution obeying the boundary conditions $p(a) = 1$ and $p(\infty) = 0$ is a spherical Hankel function of the second kind:

$$p(r) = \frac{a}{r}e^{-(r-a)/\sqrt{D\tau}} \tag{5}$$

where $l_{\mathrm{diff}} = \sqrt{D\tau}$ is the 1-D diffusion length.[23] We validated this expression with kinetic Monte Carlo simulations (see Figure S1). Substituting eq 5 into eq 1, we can compute the QY for different exciton diffusion lengths as a function of quencher number density (Figure 2). The quencher radius is considered to be 0.75 nm, which is a typical dimension for organic semiconductors.

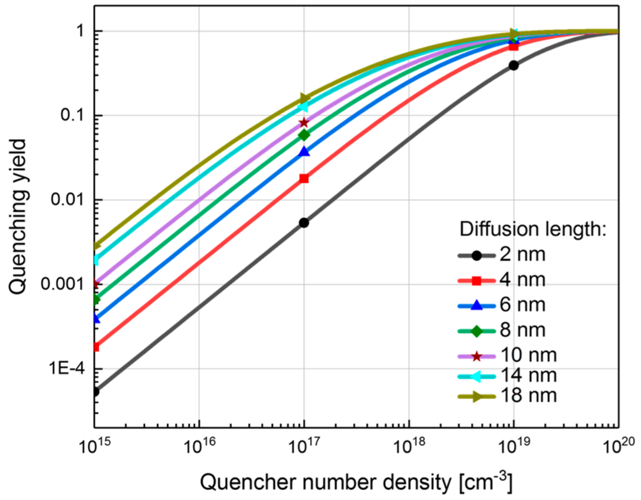

Figure 2. Predicted exciton quenching yield plotted versus the number density of quenchers for exciton diffusion lengths between 2 and 18 nm. Saturation occurs at lower concentrations for larger exciton diffusion lengths, as one would intuitively expect.

We experimentally studied two polymeric semiconductors, poly(3-hexylthiophene-2,5-diyl) (P3HT) and poly[*N*-9-heptadecanyl-2,7-carbazole-*alt*-5,5-(4′,7′-di-2-thienyl-2′,1′,3′-benzothidizole)] (PCDTBT) and a fullerene derivative [6, 6]-phenyl-C71-butyric acid methyl ester (PC70BM) for analysis with this model. In this regard, standard architecture organic solar cells with a structure ITO/PEDOT:PSS/semiconductor/Al where ITO is indium tin oxide and PEDOT:PSS is poly(3,4-ethylenedioxythiophene):poly(styrenesulfonate)] were fabricated. Notably, semiconducting active layers were prepared from solutions at different concentrations of the exciton quenching material (PC70BM for the polymers and TAPC for the fullerene) via sequential dilution where TAPC is 4,4′-cyclohexylidenebis[*N*,*N*-bis(4-methylphenyl)-benzenamine]. Further details of device fabrication and characterization are provided in the Supporting Information.

Experimental Results. We now move on to our experimental results for quantifying the exciton quenching efficiency in PC70BM, PCDTBT, and P3HT. Here we show the details of measurements on PC70BM as an example, and the results for the other two systems are presented in the Supporting Information (Figures S2 and S3). The experimental parameter that allows the evaluation of small quenching yields is the internal quantum efficiency (IQE) of the solar cells containing the three neat semiconductors with varying amounts of quencher. The IQE is the product of the exciton quenching yield, the charge transfer efficiency (η_{CT}), and the charge collection efficiency (η_{CC}):[24]

$$\mathrm{IQE} = \mathrm{QY}\eta_{\mathrm{CT}}\eta_{\mathrm{CC}} \tag{6}$$

The charge collection and transfer efficiencies in our measurements are invariant with respect to the density of quencher as all cells operate far below the charge transport percolation threshold of the quenching molecules. Hence, only those charges photogenerated very close to the electrode can be collected.[25−27] Figure 3a shows representative external quantum efficiencies (EQEs) of the low-donor-content devices measured at short circuit for PC70BM at different densities of TAPC as exciton quencher. As a matter of nomenclature, the component with the smaller electron affinity is the electron donor. By considering the parasitic absorptions and interference effects in the solar cell stack via a transfer matrix analysis, it is possible to accurately determine the IQE from this measured EQE. This is shown in Figure 3b.[28] The extinction coefficients and refractive indices of the materials of the stack are presented in Figure S4, and these were carefully determined using spectroscopic ellipsometry, Kramers−Kronig transformation, or collated from trusted literature. In order to quantify the charge generation mediated only by the quencher molecules, we subtracted the IQE of the neat (PC70BM-only) semiconductor device from all the other cells with different quencher concentrations c:

$$\mathrm{IQE}_{\mathrm{DA}}(c) = \mathrm{IQE}(c) - \mathrm{IQE}(c = 0) \tag{7}$$

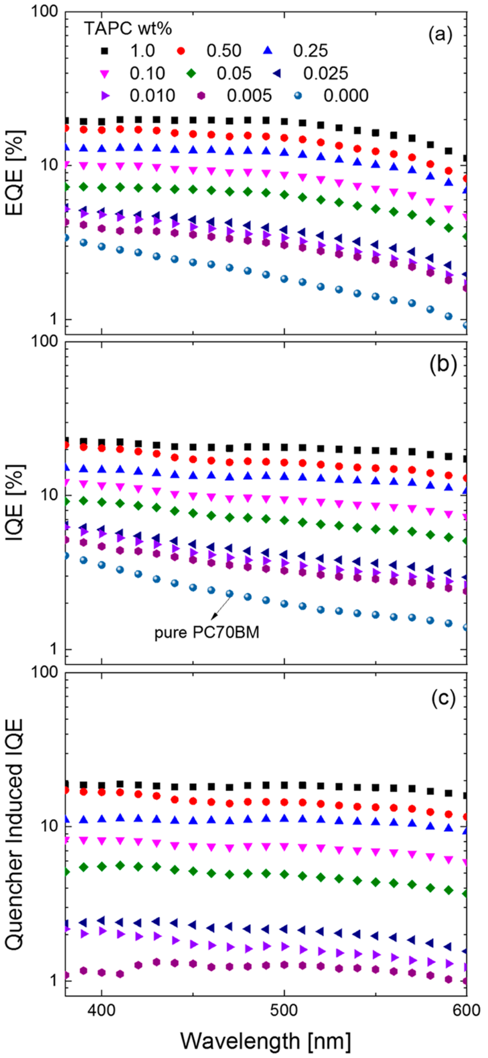

Figure 3. (a) External quantum efficiency (EQE) spectra of devices containing PC70BM as the matrix material and different concentrations of TAPC (wt %) as the quencher. (b) Internal quantum efficiency (IQE) evaluated for each device from the EQE with analysis of parasitic absorption and interference effects. At low TAPC concentrations, a wavelength-dependent IQE is observed because of wavelength-dependent (illumination energy-dependent) charge generation in predominantly neat PC70BM. (c) Quencher-induced-IQE spectra for charge generation via TAPC:PC70BM pairs evaluated by subtracting the IQE of the neat PC70BM device. These IQEs show no significant wavelength dependence.

This approach delivers the quencher-induced-IQE, $\mathrm{IQE}_{\mathrm{DA}}(c)$ in which the contribution of excitons quenched by any means other than via the quencher molecules is excluded. These contributions may arise (for example) from self-quenching within the disordered density of states of the semiconductor matrix or through trap states.[29] Quencher-induced-IQE spectra are shown in Figure 3c. They are independent of the incident illumination energy (within experimental uncertainty). This is expected for charge generation at a donor−acceptor interface, while self-quenching within the PCBM matrix ($\mathrm{IQE}(c = 0)$) is excitation energy-dependent.

The ultimate results of this analysis are shown in Figure 4 for all three systems studied (PC70BM, PCDTBT, and P3HT). The exciton quenching yield is plotted versus the number density of quenchers (calculated from the weight ratios and densities). At low quencher concentrations (<1 wt %), quenching yields were simply determined from the quencher-induced-IQEs of Figure 2c (open symbols in Figure 4). At higher quencher concentrations (>1 wt % and into the saturation regime shown in Figure 1), the QY was directly measured from steady-state PL measurements on films without the ancillary solar cell layers (filled symbols). The quencher-induced-IQE values were then normalized to match the PL data at shared quencher density data points for self-consistency. Experimental limitations precluded PL quenching measurements on the PC70BM system. However, fortunately the saturation of the QY in the fullerene was almost reached using the quencher-induced-IQEs to satisfy the model fitting. We should note that because our method probes exciton quenching using charge−carrier photogeneration, it is not confounded by long-range energy transfer from a molecule to a quencher. This mechanism has been observed in P3HT:PCBM blends.[27]

It is clear from the data in Figure 4 that the quenching yields behave differently from what would be predicted for the diffusion-only case (Figure 2). Typical diffusion lengths from 4 to 8 nm can fit the higher quencher densities $>10^{18}$ cm^{-3}. However, at lower concentrations, there is a clear anomalous trend. The exciton quenching yields are far larger than expected from an extrapolation of the diffusion-regime to low quencher densities. This secondary pathway, however, shows a linear increase at the lowest densities which saturates at mid quencher densities; this indicates the pathway is not particularly efficient. Because the exact mechanism for this quenching pathway is unclear, we cannot provide a probability function for quenching through this process that could be used in eq 1. Therefore, we used a simple and generic model suggested by Perrin[30]

$$\mathrm{QY} = 1 - \mathrm{e}^{-cV} \tag{8}$$

where c is the quencher concentration and V corresponds to the "quenching volume". The total quenching yield can then be written as the sum of the diffusion and the anomalous quenching yields

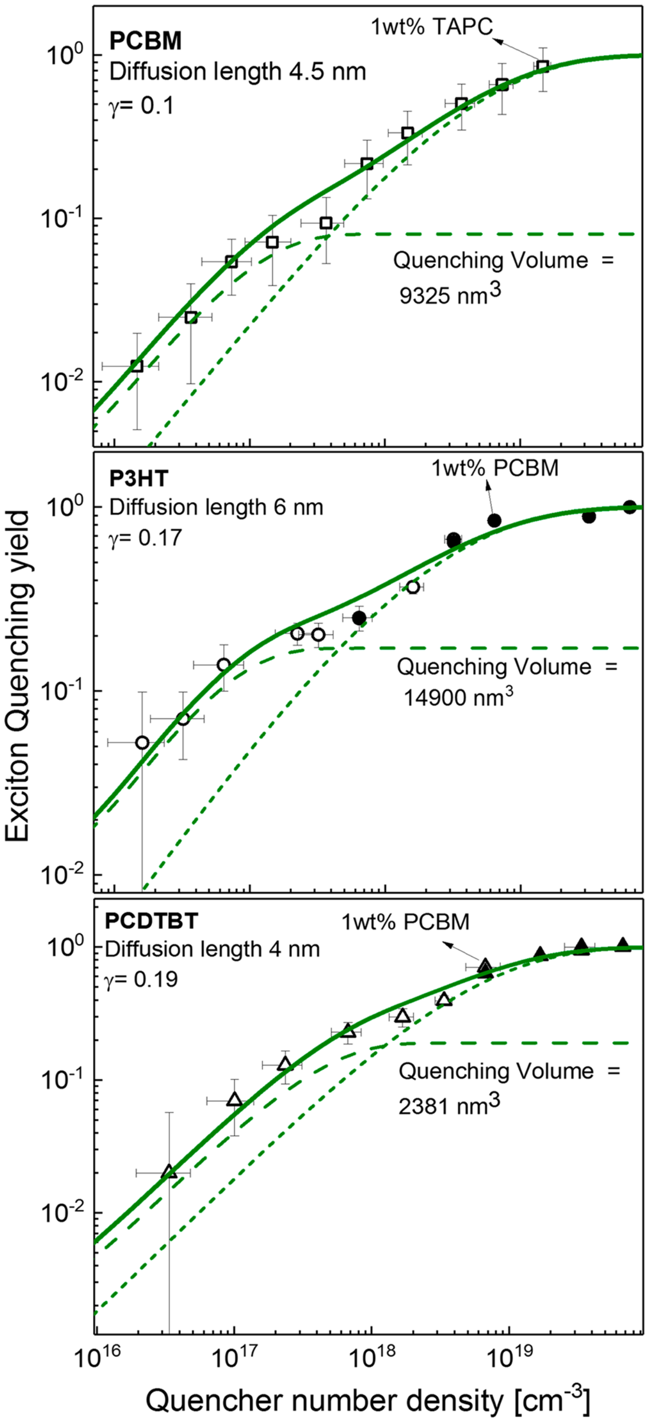

Figure 4. Exciton quenching efficiency as a function of quencher number density in PC70BM, P3HT, and PCDTBT. In all three materials, the data can be described using a steady-state exciton diffusion model at high quencher densities (dotted lines), while anomalously strong quenching is observed at low quencher concentrations (dashed lines). The solid line is a fit to eq 9, yielding exciton diffusion lengths and the quenching volume for the anomalous quenching mechanism. The vertical error bars correspond to one standard deviation of the quencher-induced-IQEs, and the horizontal error bars correspond to the concentration uncertainty calculated for sequential dilutions.

$$\mathrm{QY_{total}} = \gamma \mathrm{QY_{an}} + (1 - \gamma)\mathrm{QY_{diff}} \tag{9}$$

in which γ represents the contribution of the efficiency of the anomalous quenching pathway. The final results of the fitting based on eq 9 are shown in Figure 4 (solid lines), yielding the diffusion length and quenching volume for each material system. The values of the exciton diffusion lengths for PC70BM, PCDTBT, and P3HT are comparable to the values previously obtained using time-resolved photoluminescence.[7,15,16] The anomalous quenching pathways play a significant role in the quenching at low quencher densities, with large quenching volumes of 9 325, 14 900, and 2 381 nm^3 in PC70BM, P3HT, and PCDTBT respectively. It is plausible that such large quenching volumes may be due to delocalized excitons formed at very early times of photoexcitation within the disordered landscape, as shown recently by Mannouch et al.[31] This initially delocalized exciton can be quenched at a finite distance from the quencher prior to density localization. This pathway is not efficient and does not play a substantial role in the regime of high quencher density. Further understanding this mechanism may result in better material optimization for optoelectronic devices requiring exciton migration. The observation of a pathway with large quenching volumes is also an intriguing fundamental insight into disordered semiconductors requiring additional careful analysis.

In conclusion, we have presented a new way of measuring small exciton quenching yields based on charge photogeneration (internal quantum efficiency) measurements in the steady state. A 3-D steady-state quenching model has been developed and applied to the experimental results of quenching efficiency versus quencher density for three organic semiconductors. The exciton diffusion lengths extracted from the higher quencher density regime are consistent with previous reports using standard PL quenching methods. The improved signal-to-noise ratio of our technique is a key feature and allows for quantification of the quenching yields at low quencher densities. In this regime, we found an anomalous quenching pathway which is not efficient but long-range. This may be related to a question that has been a matter of some debate in the organic semiconductor community, namely whether exciton quenching occurs through localized or delocalized states. Our observations may be indicative of delocalized excitons being quenched at a certain distance from the quencher before they thermalize.

■ ASSOCIATED CONTENT

Ⓢ Supporting Information

The Supporting Information is available free of charge on the ACS Publications website at DOI: 10.1021/acs.jpclett.8b02484.

Experimental details, IQE spectra, optical constants, and photoluminescence data (PDF)

■ AUTHOR INFORMATION

Corresponding Authors

*E-mail: ardalan.armin@swansea.ac.uk.
*E-mail: paul.meredith@swansea.ac.uk.
*E-mail: ivan.kassal@sydney.edu.au.

ORCID

Ivan Kassal: 0000-0002-8376-0819
Ardalan Armin: 0000-0002-6129-5354

Notes

The authors declare no competing financial interest.

■ ACKNOWLEDGMENTS

This work including N.Z. was supported through the Sêr Cymru II Program "Sustainable Advanced Materials" (Welsh European Funding Office – European Regional Development Fund). P.M. is a Sêr Cymru Research Chair, and A.A. is a Sêr Cymru Rising Star Fellow. I.K. was supported by the Westpac Bicentennial Foundation and by the Australian Research Council through a Discovery Early Career Researcher Award (DE140100433). This work was performed in part at the Queensland node of the Australian National Fabrication Facility (ANFF), a company established under the National Collaborative Research Infrastructure Strategy to provide nano- and micro-fabrication facilities for Australia's researchers, and using facilities at the Centre for Organic Photonics and Electronics at the University of Queensland. We thank Dr. Safa Shoaee at the University of Potsdam for steady-state PL quenching measurements.

■ REFERENCES

(1) Brédas, J.-L.; Norton, J. E.; Cornil, J.; Coropceanu, V. Molecular Understanding of Organic Solar Cells: The Challenges. *Acc. Chem. Res.* **2009**, *42*, 1691−1699.

(2) Feron, K.; Zhou, X.; Belcher, W.; Dastoor, P. Exciton Transport in Organic Semiconductors: Förster Resonance Energy Transfer Compared with a Simple Random Walk. *J. Appl. Phys.* **2012**, *111*, 044510.

(3) Menke, S. M.; Holmes, R. J. Exciton Diffusion in Organic Photovoltaic Cells. *Energy Environ. Sci.* **2014**, *7*, 499−512.

(4) Tamai, Y.; Ohkita, H.; Benten, H.; Ito, S. Exciton Diffusion in Conjugated Polymers: From Fundamental Understanding to Improvement in Photovoltaic Conversion Efficiency. *J. Phys. Chem. Lett.* **2015**, *6*, 3417−3428.

(5) Reineke, S.; Baldo, M. A. Recent Progress in the Understanding of Exciton Dynamics within Phosphorescent OLEDs. *Phys. Status Solidi A* **2012**, *209*, 2341−2353.

(6) de Arquer, F. P. G.; Armin, A.; Meredith, P.; Sargent, E. H. Solution-Processed Semiconductors for Next-Generation Photodetectors. *Nat. Rev. Mater.* **2017**, *2*, 16100.

(7) Mikhnenko, O. V.; Blom, P. W.; Nguyen, T.-Q. Exciton Diffusion in Organic Semiconductors. *Energy Environ. Sci.* **2015**, *8*, 1867−1888.

(8) Lin, J. D.; Mikhnenko, O. V.; Chen, J.; Masri, Z.; Ruseckas, A.; Mikhailovsky, A.; Raab, R. P.; Liu, J.; Blom, P. W.; Loi, M. A.; et al. Systematic Study of Exciton Diffusion Length in Organic Semiconductors by Six Experimental Methods. *Mater. Horiz.* **2014**, *1*, 280−285.

(9) Lunt, R. R.; Giebink, N. C.; Belak, A. A.; Benziger, J. B.; Forrest, S. R. Exciton Diffusion Lengths of Organic Semiconductor Thin Films Measured by Spectrally Resolved Photoluminescence Quenching. *J. Appl. Phys.* **2009**, *105*, 053711.

(10) Leow, C.; Ohnishi, T.; Matsumura, M. Diffusion Lengths of Excitons in Polymers in Relation to External Quantum Efficiency of the Photocurrent of Solar Cells. *J. Phys. Chem. C* **2014**, *118*, 71−76.

(11) Luhman, W. A.; Holmes, R. J. Investigation of Energy Transfer in Organic Photovoltaic Cells and Impact on Exciton Diffusion Length Measurements. *Adv. Funct. Mater.* **2011**, *21*, 764−771.

(12) Markov, D. E.; Amsterdam, E.; Blom, P. W.; Sieval, A. B.; Hummelen, J. C. Accurate Measurement of the Exciton Diffusion Length in a Conjugated Polymer Using a Heterostructure with a Side-Chain Cross-Linked Fullerene Layer. *J. Phys. Chem. A* **2005**, *109*, 5266−5274.

(13) Markov, D.; Hummelen, J.; Blom, P.; Sieval, A. Dynamics of Exciton Diffusion in Poly (P-Phenylene Vinylene)/Fullerene Heterostructures. *Phys. Rev. B: Condens. Matter Mater. Phys.* **2005**, *72*, No. 045216, DOI: 10.1103/PhysRevB.72.045216.

(14) Scully, S. R.; McGehee, M. D. Effects of Optical Interference and Energy Transfer on Exciton Diffusion Length Measurements in Organic Semiconductors. *J. Appl. Phys.* **2006**, *100*, 034907.

(15) Mikhnenko, O. V.; Azimi, H.; Scharber, M.; Morana, M.; Blom, P. W.; Loi, M. A. Exciton Diffusion Length in Narrow Bandgap Polymers. *Energy Environ. Sci.* **2012**, *5*, 6960−6965.

(16) Shaw, P. E.; Ruseckas, A.; Samuel, I. D. Exciton Diffusion Measurements in Poly (3-Hexylthiophene). *Adv. Mater.* **2008**, *20*, 3516−3520.

(17) Hedley, G. J.; Ward, A. J.; Alekseev, A.; Howells, C. T.; Martins, E. R.; Serrano, L. A.; Cooke, G.; Ruseckas, A.; Samuel, I. D. Determining the Optimum Morphology in High-Performance Polymer-Fullerene Organic Photovoltaic Cells. *Nat. Commun.* **2013**, *4*, 2867.

(18) Siegmund, B.; Sajjad, M. T.; Widmer, J.; Ray, D.; Koerner, C.; Riede, M.; Leo, K.; Samuel, I. D.; Vandewal, K. Exciton Diffusion Length and Charge Extraction Yield in Organic Bilayer Solar Cells. *Adv. Mater.* **2017**, *29*, 1604424.

(19) Gélinas, S.; Rao, A.; Kumar, A.; Smith, S. L.; Chin, A. W.; Clark, J.; van der Poll, T. S.; Bazan, G. C.; Friend, R. H. Ultrafast Long-Range Charge Separation in Organic Semiconductor Photovoltaic Diodes. *Science* **2014**, *343*, 512−516.

(20) Piris, J.; Dykstra, T. E.; Bakulin, A. A.; Loosdrecht, P. H. v.; Knulst, W.; Trinh, M. T.; Schins, J. M.; Siebbeles, L. D. Photogeneration and Ultrafast Dynamics of Excitons and Charges in P3HT/PCBM Blends. *J. Phys. Chem. C* **2009**, *113*, 14500−14506.

(21) Wang, H.; Wang, H.-Y.; Gao, B.-R.; Wang, L.; Yang, Z.-Y.; Du, X.-B.; Chen, Q.-D.; Song, J.-F.; Sun, H.-B. Exciton Diffusion and Charge Transfer Dynamics in Nano Phase-Separated P3HT/PCBM Blend Films. *Nanoscale* **2011**, *3*, 2280−2285.

(22) Kaake, L. G.; Jasieniak, J. J.; Bakus, R. C.; Welch, G. C.; Moses, D.; Bazan, G. C.; Heeger, A. J. Photoinduced Charge Generation in a Molecular Bulk Heterojunction Material. *J. Am. Chem. Soc.* **2012**, *134*, 19828−19838.

(23) Berg, H. C. *Random Walks in Biology*; Princeton University Press: 1993.

(24) Rand, B. P.; Burk, D. P.; Forrest, S. R. Offset Energies at Organic Semiconductor Heterojunctions and Their Influence on the Open-Circuit Voltage of Thin-Film Solar Cells. *Phys. Rev. B: Condens. Matter Mater. Phys.* **2007**, *75*, 115327.

(25) Ward, A. J.; Ruseckas, A.; Samuel, I. D. A Shift from Diffusion Assisted to Energy Transfer Controlled Fluorescence Quenching in Polymer−Fullerene Photovoltaic Blends. *J. Phys. Chem. C* **2012**, *116*, 23931−23937.

(26) Markov, D.; Blom, P. Anisotropy of Exciton Migration in Poly (P-Phenylene Vinylene). *Phys. Rev. B: Condens. Matter Mater. Phys.* **2006**, *74*, No. 085206, DOI: 10.1103/PhysRevB.74.085206.

(27) Long, Y.; Ward, A. J.; Ruseckas, A.; Samuel, I. D. Effect of a High Boiling Point Additive on the Morphology of Solution-Processed P3HT-Fullerene Blends. *Synth. Met.* **2016**, *216*, 23−30.

(28) Armin, A.; Velusamy, M.; Wolfer, P.; Zhang, Y.; Burn, P. L.; Meredith, P.; Pivrikas, A. Quantum Efficiency of Organic Solar Cells: Electro-Optical Cavity Considerations. *ACS Photonics* **2014**, *1*, 173−181.

(29) Mikhnenko, O. V.; Kuik, M.; Lin, J.; van der Kaap, N.; Nguyen, T. Q.; Blom, P. W. Trap-Limited Exciton Diffusion in Organic Semiconductors. *Adv. Mater.* **2014**, *26*, 1912−1917.

(30) Perrin, F. Loi De Decroissance du Pouvoir Fluorescent en Fonction de la Concentration. *CR Acad. Sci.* **1924**, *178*, 1978−1980.

(31) Mannouch, J. R.; Barford, W.; Al-Assam, S. Ultra-Fast Relaxation, Decoherence, and Localization of Photoexcited States in π-Conjugated Polymers. *J. Chem. Phys.* **2018**, *148*, 034901.

DOI: 10.1021/acs.jpclett.8b02484
J. Phys. Chem. Lett. 2018, 9, 6144−6148